Idealized model simulations of barotropic flow on the Catalan shelf

Bjørn Gjevik, Halvard Moe and Atle Ommundsen

Department of Mathematics, University of Oslo, P.O.Box 1053 Blindern, Oslo, Norway.

Abstract

The effect of along shelf variation in shelf width on barotropic shelf edge flows and topographic shelf waves are investigated with a numerical model. The model topography represents a gradual transition from a narrow straight to a broader straight shelf region. It is designed primary to model the Catalan shelf on the northeastern Mediterranean coast of Spain, but the results obtained here are of general validity and will also apply to shelf flow under similar conditions elsewhere. The numerical experiments are carried out with flow imposed, both steady and oscillatory, at the upstream end of the narrow shelf region. With a prescribed shelf edge flow there is a strong tendency for topographic steering in the transition zone. The adjustment is found to take place on a short time scale of 2-5 days set by propagating wave modes rather than by advection. Bottom friction effects do not lead to significant on-shelf leakage of the flow. Flow instability and eddy formation are found to occur, even in cases where the potential vorticity for the imposed flow does not have a local maximum on the shelf slope. The instability leads to development of anticyclonic eddies on the narrow shelf which undergo strong non-linear adjustment at the transition zone from a narrow to a broader shelf. On the broad section of the shelf near the transition zone there is a tendency for formation of a large anticyclonic eddy. Bottom friction is found to influence the flow instability and the formation of eddies in cases where the flow is marginal for instability and growth of eddies. Particle tracking has been performed in order to study cross shelf mixing and transport. Finally we have studied the current response due to a concentrated wind stress jet acting perpendicular to the coast line in the transition zone between the narrow and the broad shelf regions. A dipolar eddy structure is found to develop with the axis of the dipole tilting about 30 degrees with the axis of the wind jet and with strong current shear in the zone near the dipole axis.

Key words: Numerical Model, Shelf Dynamics, Slope Currents, Topographic Steering, Mesoscale Eddies, Particle Motion, Catalan shelf

1 Introduction

The topography of the shelf in the vicinity of the Ebro Delta is characterized by the transition from a narrow shelf (width $\sim$ 10 km) north of the Delta to a broader shelf (width ~ 60 km) south of the Delta. This change in width is expected to have a profound effect on the shelf flow and on cross shelf transports. The prevailing current near the shelf break is a predominantly S to SW along shelf mean current often with a strong barotropic character of the flow in all seasons. Field measurements also indicate topographic steering of the flow along the shelf edge in the transition zone from the narrow to the broader shelf (Font, 1990, Font et al., 1990). Important mesoscale variability has been observed in the current mainly in the winter. Mesoscale eddies and filaments are also observed on satellite images and are generally believed to be associated with the density front at the shelf slope (Wang et al., 1988, Tintoré et al., 1990, La Violette et al., 1990).

In order to investigate the characteristics of the shelf sea circulation and current variability in the area near the Ebro Delta we have performed a series of model simulations under idealized conditions and results of these will be reported here. The general questions being asked are: How does bottom topography affect the steering and stability of the barotropic along shelf current? What are the processes of producing barotropic eddies and what determine their temporal and spatial scales? How are these eddies influenced by along shelf variation in shelf width? To what extent does a shelf slope current affect the flow on the shelf and how does bottom friction influence the on-shelf penetration of a slope trapped current?

Since the along shelf mean current is flowing with land on the right we have, on the Catalan shelf, a situation with adjustment of a cyclonic or prograde shelf current where the flow is in the direction of Kelvin and shelf wave propagation. This situation is typical for most northwestern European shelves as well as for many other shelf seas areas. Along shelf variation in shelf width, similar to what occur outside the Ebro Delta, is also a common shelf feature. Although the simulations reported here primarily are designed for application to shelf near the Ebro Delta the results obtained will also shed light on flow adjustment due to along shelf variation in shelf topography in other shelf seas. Mesocale flows, generated by adjustment of prograde mean current over topographic features, have recently been studied by several authors; Willmot and Collings (1994), Gjevik and Moe (1994), and Yankovsky and Chapman (1997). However, none of these have addressed flow associated with the bottom topography typical for the Catalan shelf.

The shelf and shelf flow are characterized with the following parameters; shelf width L, shelf slope $\alpha = \mid \frac{dH}{dy} \mid$ where H is the depth and y the cross shelf coordinate, mean along shelf current speed $\overline{u}$, and the current shear $\beta = \mid \frac{d\overline{u}}{dy} \mid$. Based on the two gradient parameters we introduce a shelf slope width $S = H/\alpha$ and a width of current shear zone $B = \overline{u}/\beta$ with typically $S \sim B$. For the narrow shelf north of the Delta $L < S$ while $L \sim S$ for the broad section of the shelf. The lowest mode barotropic shelf waves have phase velocity of order fL (f is the Coriolis parameter) and the Rossby number $Ro = \frac{\overline{u}}{fL}$, i.e. the ratio between advection velocity $\overline{u}$ and shelf wave speed, measures

the nonlinear effects on the flow. For the narrow section of the shelf Ro is of order from $O(10^{-1})$ to $O(1)$, indicating a relatively strong nonlinear effect on the flow. For the broad section of the shelf Ro is of order from $O(10^{-2})$ to $O(10^{-1})$ with a corresponding weaker effect of nonlinearity. Cross shelf current speed $\overline{v}$ and wave period T define the cross shelf particle excursion distance, $D = \overline{v}T$, with $D \sim L$ at least for for the narrow section of the shelf. Unstable growing modes with possible eddy formation may emerge in the along shelf slope current if the Rossby number $Ro = \frac{\overline{u}}{fB}$, based on the width of the current shear zone, is of order $O(10^{-1})$ and with $\frac{B}{S}$ of order $O(1)$ or smaller. These conditions are expected to be satisfied with both on the narrow and the broad section of the shelf indicating that unstable barotropic modes are an important mechanism for eddy generation in the shelf flow.

The effects of longshore variation in the width of the shelf and the shelf slope on the propagation of shelf waves have previously been studied by Huthnance (1987), Webster (1987) and Wilkin and Chapman (1987). The shelf topography and wave parameter range examined in these papers do not cover the Catalan shelf and their results therefore have little relevance for this case.

Compared to most northwest European shelves the Catalan shelf near the Ebro Delta is a narrow shelf in the sense that cross shelf particle excursion in the shelf wave motion is of the order of the shelf width. The characteristic Rossby numbers, based either on the shelf width or the width of the shear zone in the along shelf mean current, are also larger than for most northwest European shelves. This indicates that nonlinear effects and flow instability are important for the Ebro Delta shelf. The results obtained here therefore extend earlier studies of flow adjustment in the transition zone between narrow and broader sections of a shelf (Huthnance, 1987, Haugan et al., 1991).

2 Model Description

We apply a barotropic ocean model with an incompressible and homogeneous fluid with density ρ. A Cartesian coordinate system (x, y, z) is introduced with the x and y-axis horizontal in the level of the undisturbed surface and the z-axis vertical. We assume that the flow has a sufficiently large horizontal length scale so that hydrostatic pressure distribution applies. The depth integrated equations of motion can therefore be written;

$$\frac{\partial U}{\partial t} - fV + \frac{\partial}{\partial x}\left(\frac{U^2}{H+\eta}\right) + \frac{\partial}{\partial y}\left(\frac{UV}{H+\eta}\right) = -g(H+\eta)\frac{\partial \eta}{\partial x} + \frac{\tau_{sx}}{\rho} - \frac{\tau_{bx}}{\rho} + A_x \qquad (1)$$

$$\frac{\partial V}{\partial t} + fU + \frac{\partial}{\partial x}\left(\frac{UV}{H+\eta}\right) + \frac{\partial}{\partial y}\left(\frac{V^2}{H+\eta}\right) = -g(H+\eta)\frac{\partial \eta}{\partial y} + \frac{\tau_{sy}}{\rho} - \frac{\tau_{by}}{\rho} + A_y \qquad (2)$$

and conservation of mass implies

$$\frac{\partial \eta}{\partial t} = -\frac{\partial U}{\partial x} - \frac{\partial V}{\partial y} \tag{3}$$

Here U and V are respectively the x and y components of the horizontal volume flux, H is the undisturbed depth, η denotes the vertical displacement of the surface, g is the acceleration of gravity, and t is time. The components of the shear stresses at the surface and the sea bed are (τ_{sx}, τ_{sy}), (τ_{bx}, τ_{by}) respectively. The terms A_x and A_y represent the stress associated with horizontal eddy viscosity parameterized by;

$$A_x = \nu \bigtriangledown^2 U$$

$$A_y = \nu \bigtriangledown^2 V$$

where $\bigtriangledown^2$ is the horizontal Laplace operator. The eddy viscosity ν is given according to Smagorinsky (1963)

$$\nu = ql^2[(\frac{\partial \overline{u}}{\partial x})^2 + \frac{1}{2}(\frac{\partial \overline{u}}{\partial y} + \frac{\partial \overline{v}}{\partial x})^2 + (\frac{\partial \overline{v}}{\partial y})^2]^{\frac{1}{2}} \tag{4}$$

where $(\overline{u}, \overline{v})$ denote the components of the depth mean current velocity defined to first order by;

$$\overline{u} = \frac{U}{H}, \quad \overline{v} = \frac{V}{H}$$

q is a constant and l is a length scale which is set equal to the grid size. With q=0.1, a grid size of 1 km, and current speed of the order 0.1 m/s eq. 4 leads to an eddy viscosity of the order 10 m^2/s In some simulations we have also applied a spatial constant horizontal eddy viscosity with ν ranging from 1 to 10 m^2/s instead of the flow dependent viscosity (4).

The shear stresses at the sea bed (τ_{bx}, τ_{by}) are modelled by a quadratic friction law:

$$\tau_{bx} = -\rho r_b \overline{w}\, \overline{u}, \quad \tau_{by} = -\rho r_b \overline{w}\, \overline{v} \tag{5}$$

where r_b is the bottom drag coefficient and

$$\overline{w} = (\overline{u}^2 + \overline{v}^2)^{\frac{1}{2}}$$

is the depth mean current speed.

Lagrangian motion of particles released in the current field is found by integrating the equations

$$\frac{dx_k}{dt} = \overline{u}(x_k, y_k, t) \quad \frac{dy_k}{dt} = \overline{v}(x_k, y_k, t) \tag{6}$$

Subscript k denotes the particle number ($k = 1 \ldots M$), and (x_k, y_k) its position. The particle tracking algorithm is incorporated in our barotropic model. We have used a standard Euler forward time stepping as initiator combined with an Adams-Moulton method for the numerical integration of the equations (6). The integration is performed with the time step used in the ocean model, and the depth mean current in position (x_k, y_k) is obtained by bilinear interpolation from the four closest current nodes.

The initiator should in principle have an accuracy comparable to the Adams-Moulton method. For convenience we used the Euler method despite its low accuracy. The error introduced by the initiator is negligible because the currents are very small at the time of particle release.

This particle tracking technique is computational effective, captures the mesoscale phenomena resolved by the barotropic model in space and time and also enables the possibility of tagging each particle with specific attributes such as age and initial depth of release.

3 Model domain and shelf topography

The model domain has the form of a rectangular channel (fig. 1) with dimensions (L_x, L_y) respectively in the x and y directions and with open boundaries at the upstream ($x = 0$) and downstream ($x = L_x$) ends. In most simulations we have used $L_x =$ 300 km and $L_y = 150$ km, but in order to investigate the effects of boundary conditions on the interior solution we have also performed simulations with an enlarged domain.

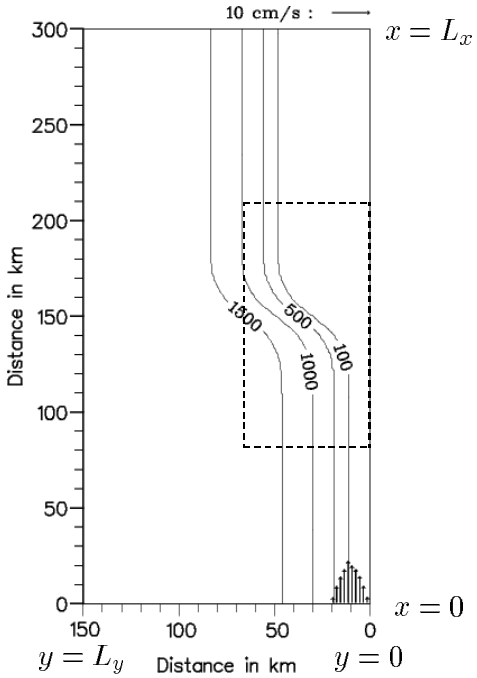

Figure 1. Model domain and jet profile at upstream boundary. Subdomain for current fields shown in subsequent figures is marked by dotted lines.

In order to be able to perform a systematic study of the effect of topography on

shelf flow we have used idealized shelf topography models which capture the main characteristics of the Catalan shelf near the Ebro Delta area. On the shelf depth, H, increases linearly from H_C at the coast, $y = 0$, to H_S at the self break, $(y = L)$. The shelf slope profile can be approximated by a parabolic function with uniform depth, H_0, off the shelf

$$\begin{aligned} H &= H_C + \frac{H_S - H_C}{L} y && 0 < y < L \\ H &= H_0 - (H_0 - H_S)\left(\frac{L + S - y}{S}\right)^2 && L \leq y \leq L + S \\ H &= H_0 && L + S < y < L_y \end{aligned} \tag{7}$$

which fits well to the actual shelf profile (fig. 2). We have also in some cases used a sine shelf slope profile

$$H = \frac{H_0 + H_S}{2} + \frac{H_0 - H_S}{2} \sin \frac{\pi(y - L - \frac{S}{2})}{S} \qquad L < y < L + S \tag{8}$$

The along shelf variation in shelf width is modelled by

$$L(x) = L_0 + \frac{L_D - L_0}{2}\left[1 + \tanh \frac{2(x - x_0)}{L_T}\right] \tag{9}$$

where L_0, and L_D are the upstream and downstream width of the shelf respectively, and L_T is the length of the transition zone. The center of the transition zone is located at the along shelf coordinate $x = x_o$. At the upstream and downstream boundaries of the model domain $\mid \frac{2(x-x_0)}{L_T} \mid \gg 1$. Standard parameter choices for the shelf profile are given in table 1.

4 Boundary and initial conditions

At the side walls of the channel we have used zero normal volume flux at the coastal boundary $(y = 0)$ and at the oceanic boundary $(y = L_y)$. At the open boundary at the upstream end of the channel $(x = 0)$ we have specified the depth mean current as a along shelf barotropic jet centered at $y = L_B$ with cosine profile defined by:

$$\overline{u} = \frac{u_o s(t)}{2}\left[1 + \cos \frac{2\pi(y - L_B)}{B}\right] \qquad L_B - \frac{B}{2} < y < L_B + \frac{B}{2} \tag{10}$$

where the function $s(t)$ describes the transient start. Two modified versions of the jet profile are also used; a jet with a cosine profile without inflection points:

$$\overline{u} = u_o s(t) \cos \frac{\pi(y - L_B)}{B} \qquad L_B - \frac{B}{2} < y < L_B + \frac{B}{2} \tag{11}$$

Table 1
Standard values of model parameters.

Model domain	L_x	300 km
	L_y	150 km
Grid size	$\Delta x = \Delta y$	1 km
Shelf profile		
(eq. 7)	H_C	25 m
	H_S	100 m
	H_0	1800 m
	L_0	10 km
	L_D	50 km
	S	60 km
	L_T	30 km
	x_0	150 km
Coriolis parameter	f	$0.9{\cdot}10^{-4}$ s^{-1}
Bottom friction	r_b	0.003
Horizontal eddy	q	0.1
viscosity parameter		
Time factor for	σ	$2.3{\cdot}10^{-5}$ s^{-1}
transient start		

and a jet with a Gaussian profile:

$$\overline{u} = u_o s(t) \exp\left[-\left(\frac{2(y - L_B)}{B}\right)^2\right] \tag{12}$$

The second type of profile has uniform along shelf current on the shelf with a sine shear layer over the shelf slope with current velocity decaying to zero in the deep ocean.

$$\begin{aligned} \overline{u} &= u_o s(t) && 0 < y < L_B \\ \overline{u} &= \frac{u_o s(t)}{2}\left[1 - \sin\frac{\pi(y - L_B - \frac{B}{2})}{B}\right] && L_B < y < L_B + B \\ \overline{u} &= 0 && y > L_B + B \end{aligned} \tag{13}$$

The inflow at the boundary $x = 0$ is started from rest at $t = 0$ growing in strength according to

$$s(t) = [1 - \exp(-\sigma t)]\,[1 + p \sin \omega t] \tag{14}$$

with $\sigma = 2.3{\cdot}10^{-5}$ s^{-1} the inflow attains nearly a constant value after about 24 hours. The oscillary part of $s(t)$ is used for simulation of a modulated mean current where p defines the amplitude and ω the frequency of the perturbation. Pulse inflow events are modelled by:

$$s(t) = \sigma t \exp(1 - \sigma t) \tag{15}$$

where $\frac{1}{\sigma}$ is a typical time scale for the duration of the pulse event.

In the experiments with shelf wave propagation we have calculated the period and the modal structure of the shelf wave, surface displacement and current, and used this as upstream boundary conditions.

Boundary conditions at the downstream end $x = L_x$ should preferably be transparent to motion generated within the computational domain a condition which is difficult to obtain in numerical models (Chapman, 1985). At the downstream end we have tried different boundary conditions combined with a flow relaxation scheme (FRS) in order to relax the interior solution to the exterior i.e. the boundary conditions (Martinsen and Engedahl, 1987). The FRS is used also at the upstream boundary and in some case also at the oceanic side wall ($y = L_y$) of the channel. More details on the boundary conditions are given in the sections below where the results of the various numerical experiments are presented.

5 Grid systems and numerical methods

The set of non-linear differential equations (1-3) are discretized on a space staggered B-grid and integrated numerically with an explicit finite difference scheme which is essentially a forward-backward procedure with modifications for the advective terms. The stability and the performance of the scheme for shelf sea response problems are discussed by Gjevik (1991). For comparison we have also used forward-backward scheme for the linear part of the differential operator with an iterative scheme similar to the Heun scheme (Mesinger and Arakawa, 1976) for the non-linear advective terms, and also a standard leap-frog scheme.

Most of the simulations are made with a grid resolution of 1 km, but in several cases we have performed grid refinements test by decreasing the grid size to half. These test refinements show that the mesoscale phenomena considered here are well resolved by the standard grid resolution. The horizontal eddy viscosity model (eq. 4) is implemented only at interior points where central differencing can be made. Hence, there will essentially be a slip boundary condition applied at the grid point near the coastline. This is not found to have any noticeable effects on the interior solution.

With the animation graphic package GASP (from Florida State University) we have produced animations of several simulated current fields. The animation sequences of potential vorticity display the development and propagation of waves and eddies in the along shelf slope current and their interaction with bottom topography. This technique has been commonly used for error diagnosis and interpretation of the results.

6 Shelf wave oscillations

The topography of the Catalan shelf favours shelf wave dynamics (Mysak, 1980, Huthnance, 1981, 1995) with different characteristics for the narrow and broad sections of the shelf respectively. Assuming a along shelf propagating harmonic linear wave component; the governing differential equations for the cross shelf wave profile are integrated numerically with a fourth order Runge-Kutta method (Press et al., 1989). The corresponding eigenvalue, i.e wave speed and period, is determined by a shooting technique. The method works well for most cross shelf depth profiles including also a along shelf steady current which may vary in strength in cross shelf direction. The error in the calculated period is usually less than 1%.

Results of the calculations of the dispersion properties for shelf waves on two typical idealized depth profiles, one for the narrow, the second for the broad section of the Catalan shelf are shown in fig. 2. A characteristic difference in dispersion properties between the narrow and the broad sections of the shelf is demonstrated clearly. Northeast of the transition zone, where the shelf is narrow, barotropic shelf waves will have period larger than about 30 hours. Phases will propagate downstream, south-westwards, with phase speed about 1 m/s for the lowest mode. Group velocity and energy transport will be in the same direction for wavelengths larger than about 50 km while shorter wave components will propagate energy upstream. Southwest of the transition zone, where the shelf is broader, barotropic shelf waves will have periods down to about 24 hours. Phases will propagate downstream with phase speed about 1 m/s for the lowest mode. For the wave with minimum period, $T_m \sim 24$ hours, and corresponding wavelength, $\lambda_m \sim 140$ km, group velocity is zero. For wavelength $\lambda > \lambda_m$ group velocity and phase speed are in the same direction i.e. downstream energy flux while for $\lambda < \lambda_m$ group velocity and phase velocity have opposite sense i.e. upstream energy flux. Hence we will have the situation that shelf wave components with wavelength of the order of 50–140 km will propagate energy towards the transition zone from both the narrow and broad sections of the shelf leading to an accumulation of wave energy. This may be a contributing factor to the development of eddies and filaments frequently observed in this area (Wang et al., 1988, Tintoré et al., 1990) although baroclinic processes may be of prominent importance.

The modal structure of the shelf wave is shown by plots of the along shelf and cross shelf current components in fig. 3. The current vector rotates anticyclonically (clockwise) on the shelf and cyclonically for distances from the coast larger than about 52 km i.e. beyond the shelf break.

An along shelf steady current will introduce a Doppler shift of shelf wave oscillation towards shorter period (Narayanan and Webster, 1987). We have calculated this effect for a shelf edge jet with a Gaussian current profile (eq. 12) with the center of the jet located near the shelf break. The wave period is reduced to 20–22 hours in the wave band 88–150 km. Below $\lambda = 88$ km the current modified shelf wave mode ceases to exist. Density stratification may also have the effect of reducing the period of shelf waves, (Kajiura, 1974, Mysak, 1980).

During the FANS field cruise in November 1996 an episode with regular current oscillations with period about 19.7 hours were observed at a station (F2), located

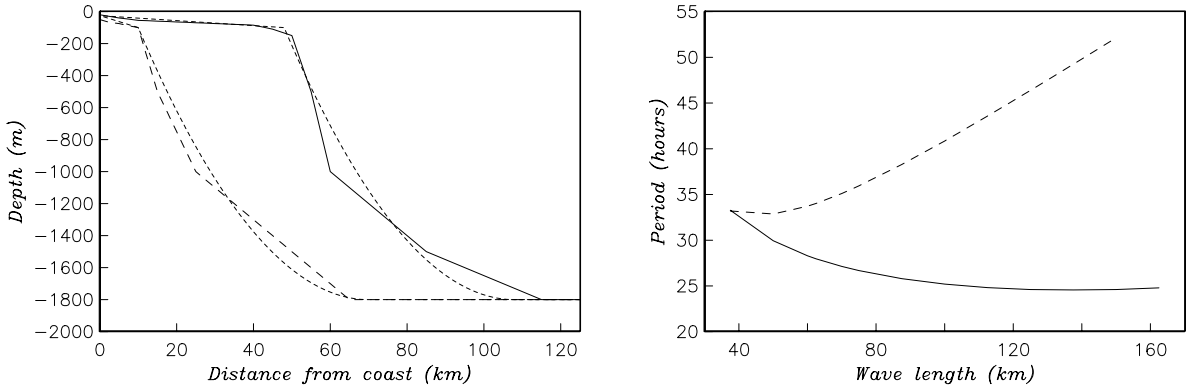

Figure 2. Typical depth profiles from the Catalan shelf (left) for the broad (full drawn) and narrow sections (coarse dotted) of the shelf. Approximated parabolic profiles, from eq. (7) with standard parameter values (table 1), fine dotted. Dispersion diagrams for first mode barotropic shelf waves for the same depth profiles (right). Narrow shelf dotted, broad shelf full drawn

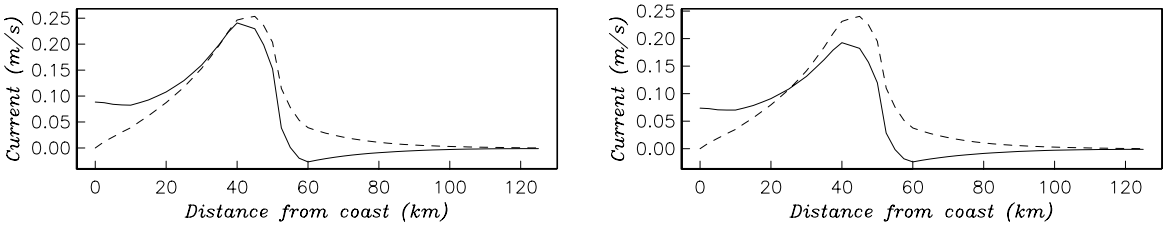

Figure 3. Modal structure for barotropic shelf waves on the broad section of Catalan shelf. Along shelf current component (full drawn) cross shelf current component (dotted). Wave length 100 km. Left; without along shelf mean current, period 25.1 hours. Right; with along shelf jet eq. (12), period 20.8 hours with $u_0 = 0.25$ m/s, L_B=45 km, B= 40 km.

at the shelf break at 90 m depth, on the broad section of the shelf, about 50 km southeast of the Ebro Delta. The oscillations continued for 5-6 days and were recorded 10 m above the sea bed (García et al., 1997). The near bottom motion indicates that the oscillations may be a manifestation of shelf wave activity. The combined effect of mean along shelf current and density stratification may reduce the period of the waves to match the observation. Unfortunately the field data do not allow the modal structure to be determined and it therefore remains an open question whether the observed oscillations are due to inertial motion or shelf waves. Inertial oscillations have previously been observed in the same area, Salat et al., (1992). Analysis of data from the FANS field campaigns in March-May 1997 (Rippeth et al. , 2000) also show strong oscilltions in the diurnal-inertial band. In these cases the vertical structure reveals a persistent phase shift of about 180 degrees between surface and near-bed velocities.

We have also investigated the propagation of shelf waves past the transition zone between the narrow and the broad shelf with the numerical model using the standard model setup in table 1, but with a larger model domain ($L_x = 300$ km, $L_y = 600$ km, $x_0 = 300$ km) in order to reduce the effect of downstream boundary conditions. In the experiments we specify a current field, periodic in time, at the upstream boundary and study the downstream propagation of the wave. Input data for spatial variation of the current i.e. the modal structure of the wave, are obtained with the method described

earlier in this section. At the downstream boundary we relax the solution towards zero, thus absorbing the energy in a flow relaxation layer using the FRS method.

Results of two illustrating experiments are shown in figs. 4 and 5. In the first case (fig. 4) the period and current structure specified at the upstream boundary correspond to lowest mode shelf wave with period 33.1 hours close to the minimum period for this section of the shelf (fig. 2). We see that the wave propagates downstream towards the transition zone with phase speed about 0.45 m/s and a wave length of about 53 km. The wave signal disappear after the transition in shelf width since the broader shelf does not support shelf waves with this short period and the wave signal is apparently scattered into rapidly decaying evanescent modes at the transition zone.

In the second case (fig. 5) the period and current structure specified at the upstream boundary correspond to lowest mode shelf wave with period 24.5 hours, close to the minimum period for the broad downstream section of the shelf (fig. 2). On the narrow shelf the oscillating current signal is very weak, but it is amplified strongly due to resonance near the transition zone. A shelf wave is generated with the forced period which propagates downstream with phase speed about 1.6 m/s and a wave length of about 130 km. The strongest current is confined to the shallow shelf and with the distinct character of a single mode shelf wave.

7 Topographic steering

A strong tendency for topographic steering of the flow along the steeper part of the shelf slope in the transition zone from the narrow to the broader shelf is evident in all simulations.

In the numerical experiments topographic steering of the flow develops over a time scale of 2-5 days after the inflow event started on the upstream boundary. This is considerable shorter than the advection time with peak mean current from the upstream boundary to the transition zone. This shows that the adjustment to topographic steering takes place on a shorter time scale set by propagating wave modes.

The effect of on-shelf leakage of a steady barotropic slope-trapped current due to bottom friction has previously been pointed out by several authors. Based on linearized steady state equations Hill (1995) defined a leakage length scale which with parameters typical for the Catalan shelf is found to be of the order 100 km. We find here, with inertial effects included, that bottom friction reduces the flow level on the shelf and prevents formations of eddies, a process makeing topographic steering a more prominent feature of the simulated current fields. This important effect is an inherent character of transient development of the flow on the shelf missed by previous studies of the effect of bottom friction limited to steady state situations.

Three typical examples of topographic steering are shown in figs. 6-8 with different current profiles imposed at the upstream boundary. The inflow events are initiated according to eq. (14) with p=0. In the first case the inflow is specified as a relatively broad jet centered on the shelf edge. With bottom friction the flow is stable and the steering along the shelf edge is evident already after 5 days and becomes gradually more pronounced after 10 and 15 days (fig. 6, upper panels). The flow on the broad

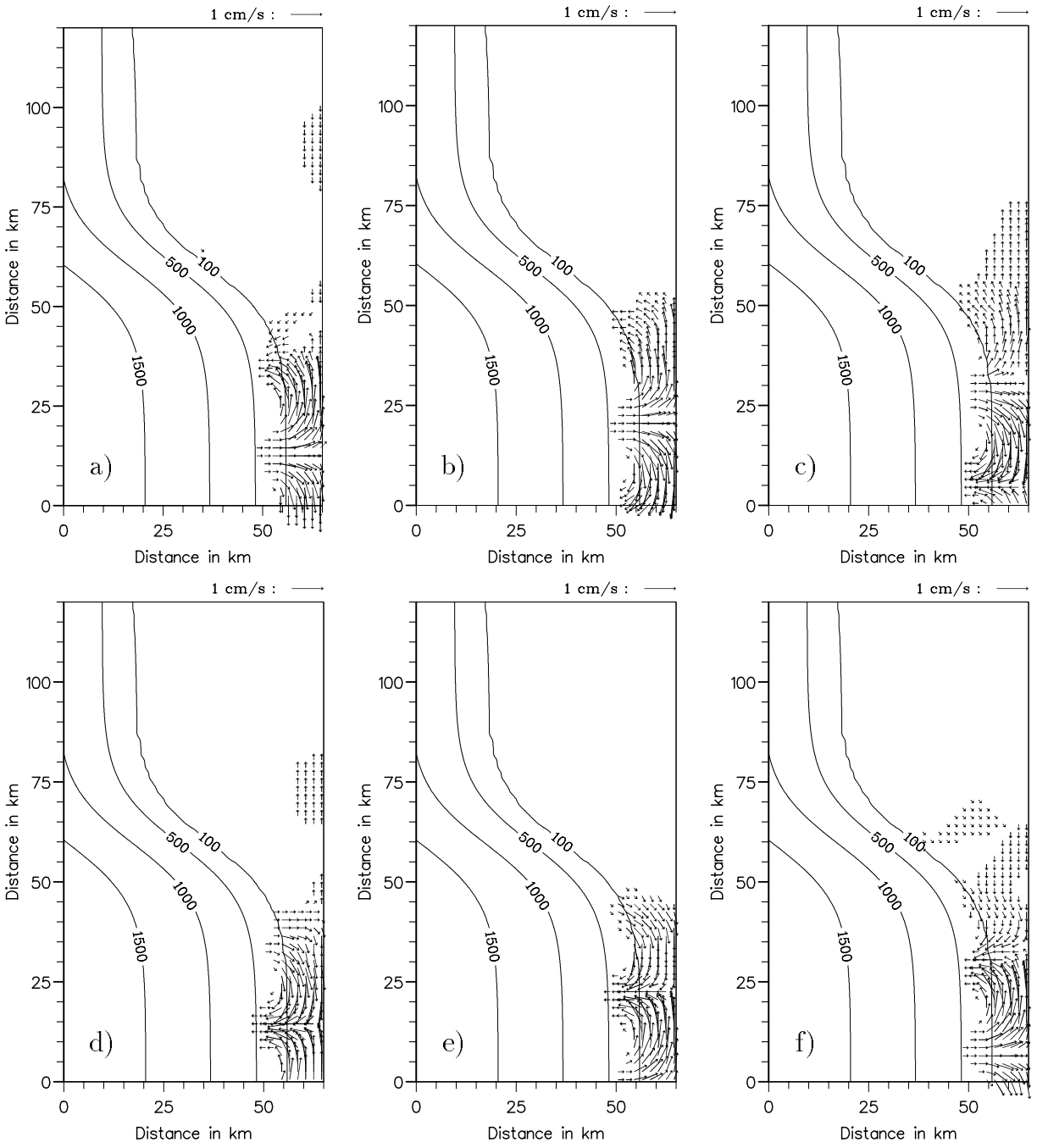

Figure 4. Shelf wave on narrow section of the shelf. Input at upstream boundary corresponding to lowest mode barotropic shelf wave with period $T = 33.1$ hours. Plots of current fields at consecutive intervals of 6 hours respectively from day 25, ordered left-right top-bottom.

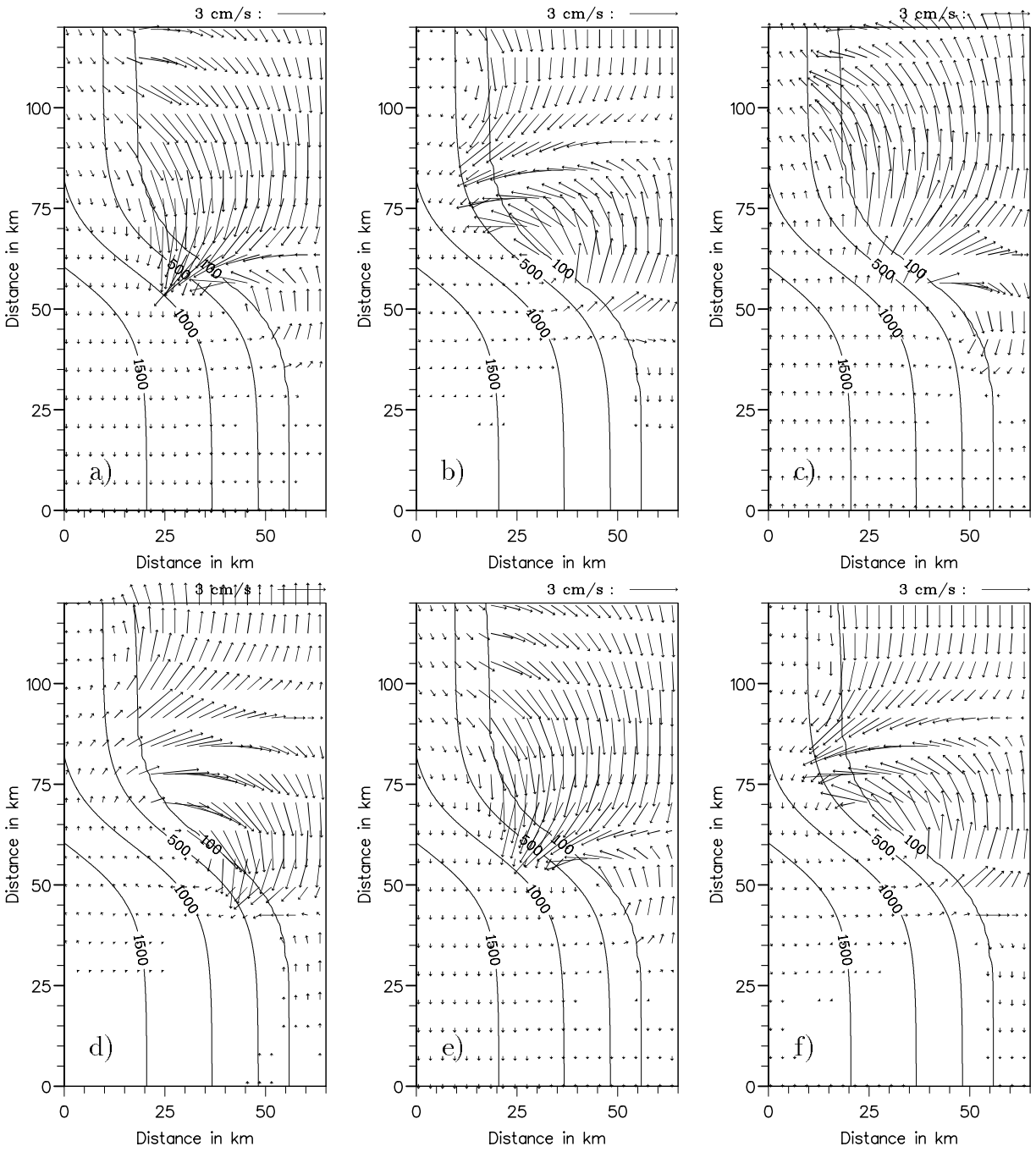

Figure 5. Shelf wave on broad section of the shelf. Periodic flow input at upstream boundary with period T= 24.5 hours corresponding to lowest mode shelf wave on the broad section of the shelf. Plots of current fields at consecutive intervals of 6 hours respectively from day 25, ordered left-right top-bottom.

section of the shelf, downstream from the transition zone, is much weaker compared to the flow along the steep part of the shelf slope. Without bottom friction (lower panels) the flow becomes unstable with a strong tendency for eddy formation particularly after 10-15 days. This changes the character of the flow on the broader section of the shelf fundamentally compared to the situation with bottom friction. Albeit the cross shelf flows are induced by the eddies the tendency to topographic steering along the steep part of the shelf slope is still pronounced.

In the second case the inflow at the upstream boundary is specified as a narrow jet centered on the shelf slope (fig. 7). This leads to a strong tendency for topographic steering along the steeper part of the shelf slope with a relatively weak currents on the broad section of the shelf, particularly when bottom friction is included (upper panels). Without bottom friction we see the same tendency as in the previous case to flow instability with formation of eddies which induce stronger currents and more current variability on the shelf. The effect of topographic steering of the flow is, however, still prominent. Further details on the development of eddies in this case are shown in fig. 10 and are also discussed in the next section.

The third case considers inflow at the upstream boundary in the form of a uniform current on the shelf with the current tapering off to zero in a sine shear layer over the shelf slope (fig. 8). Also in this case the effect of topographic steering is pronounced particularly with bottom friction and we see again the tendency for flow instability and eddy formation with strong currents and current variability on the shelf when bottom friction is not included.

Plots of potential vorticity (not shown here) demonstrate clearly the topographic steering and also the intrusion of water from the shelf edge onto the broader section of the shelf associated with the formation of eddies. The mechanism of flow instability and eddy formation is discussed in more details in section 8.

It is also interesting to note that the profile of the shelf edge current in the transition zone attains a characteristic skewness with a rapid increase in current speed near the shelf edge towards a maximum on the steeper part of the slope and a gradual tapering off on the seaward side.

8 Instability of along shelf current and development of eddies

A necessary condition for an instability of an inviscid barotropic along shelf current is that the potential vorticity

$$Q = \frac{f - \frac{d\overline{u}}{dy}}{H} \tag{16}$$

has a maximum which implying that

$$\frac{dQ}{dy} = \frac{1}{H}\left[\kappa\left(\frac{d\overline{u}}{dy} - f\right) - \frac{d^2\overline{u}}{dy^2}\right] \tag{17}$$

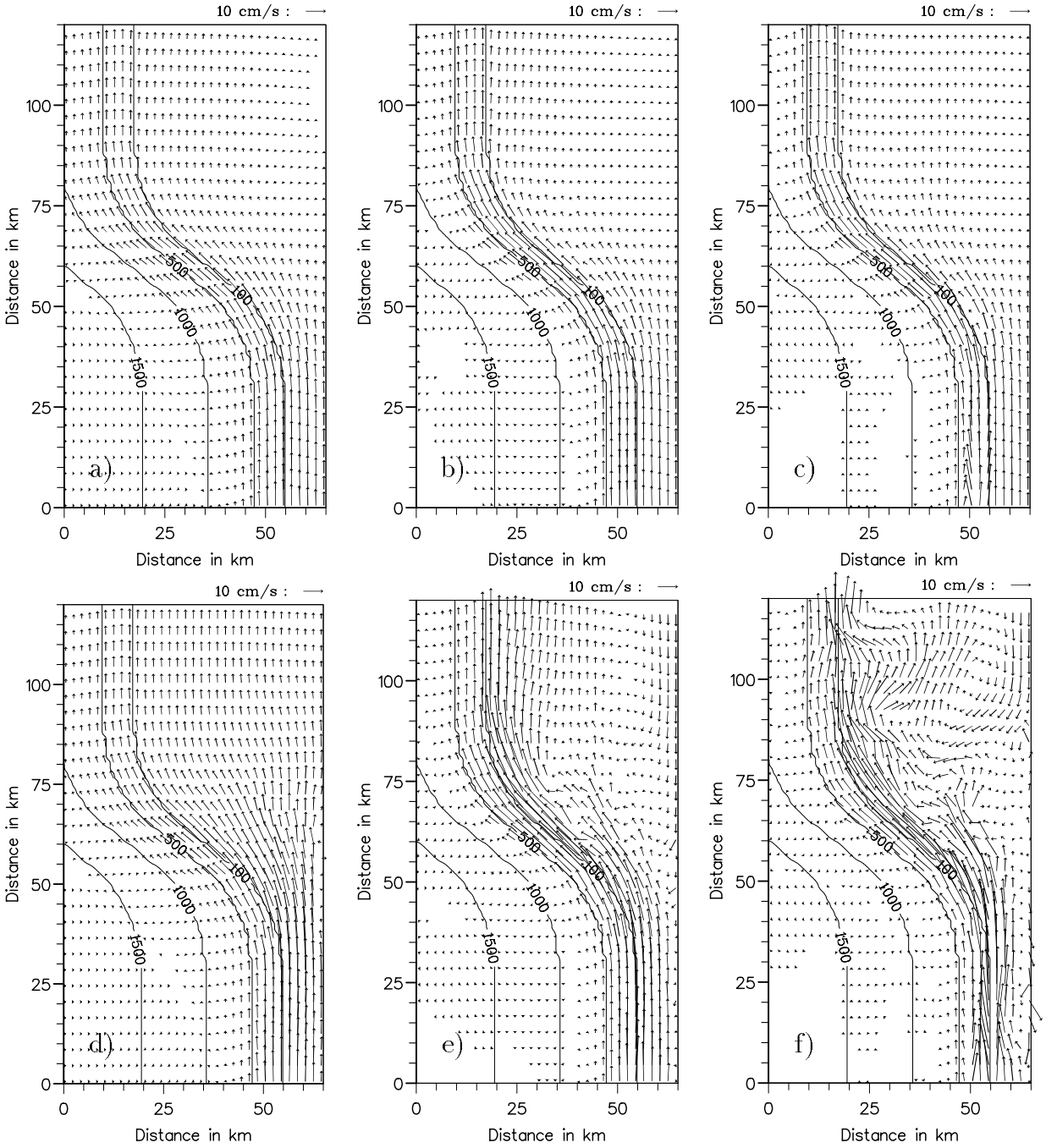

Figure 6. Topographic steering of a wide jet centered at shelf break (eq. 11) with $u_0 = 0.2$ m/s, $B = 20$ km , L_B= 10 km. Shelf slope profile (eq. 7) with standard parameter values (table 1). Current fields near the transition zone at time 5, 10 and 15 days respectively left to right. Depth contours for 100, 500, 1000 and 1500 m. Upper panel with bottom friction. Lower panel without bottom friction.

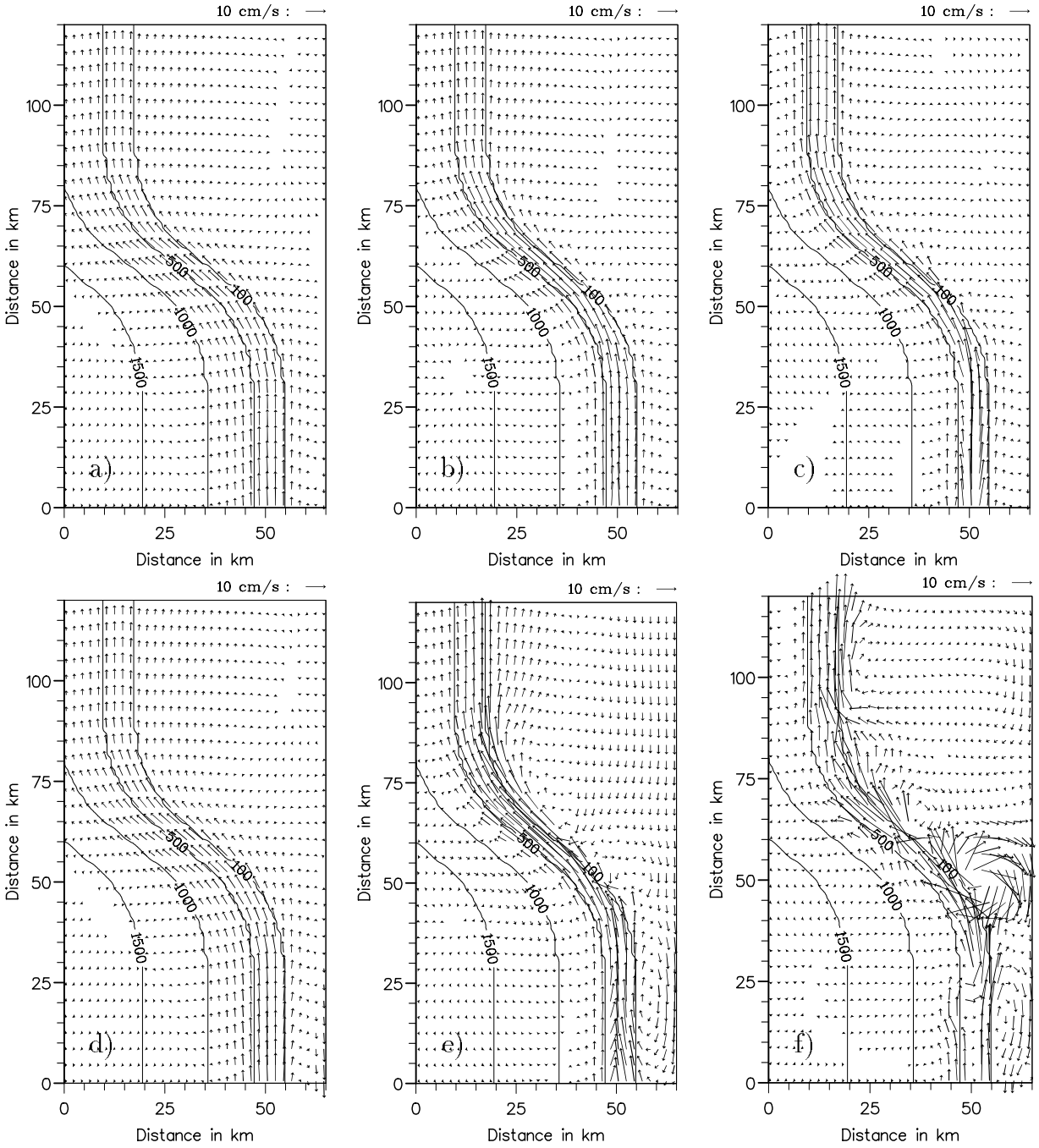

Figure 7. Topographic steering of a narrow jet centered 5 km outside shelf break (eq. 11) with $u_0 = 0.2$ m/s, $B = 10$ km, $L_B = 15$ km. Shelf slope profile (eq. 7) with standard parameter values (table 1). Current fields near the transition zone at time 5, 10 and 15 days respectively left to right. Depth contours for 100, 500, 1000 and 1500 m. Upper panel with bottom friction. Lower panel without bottom friction.

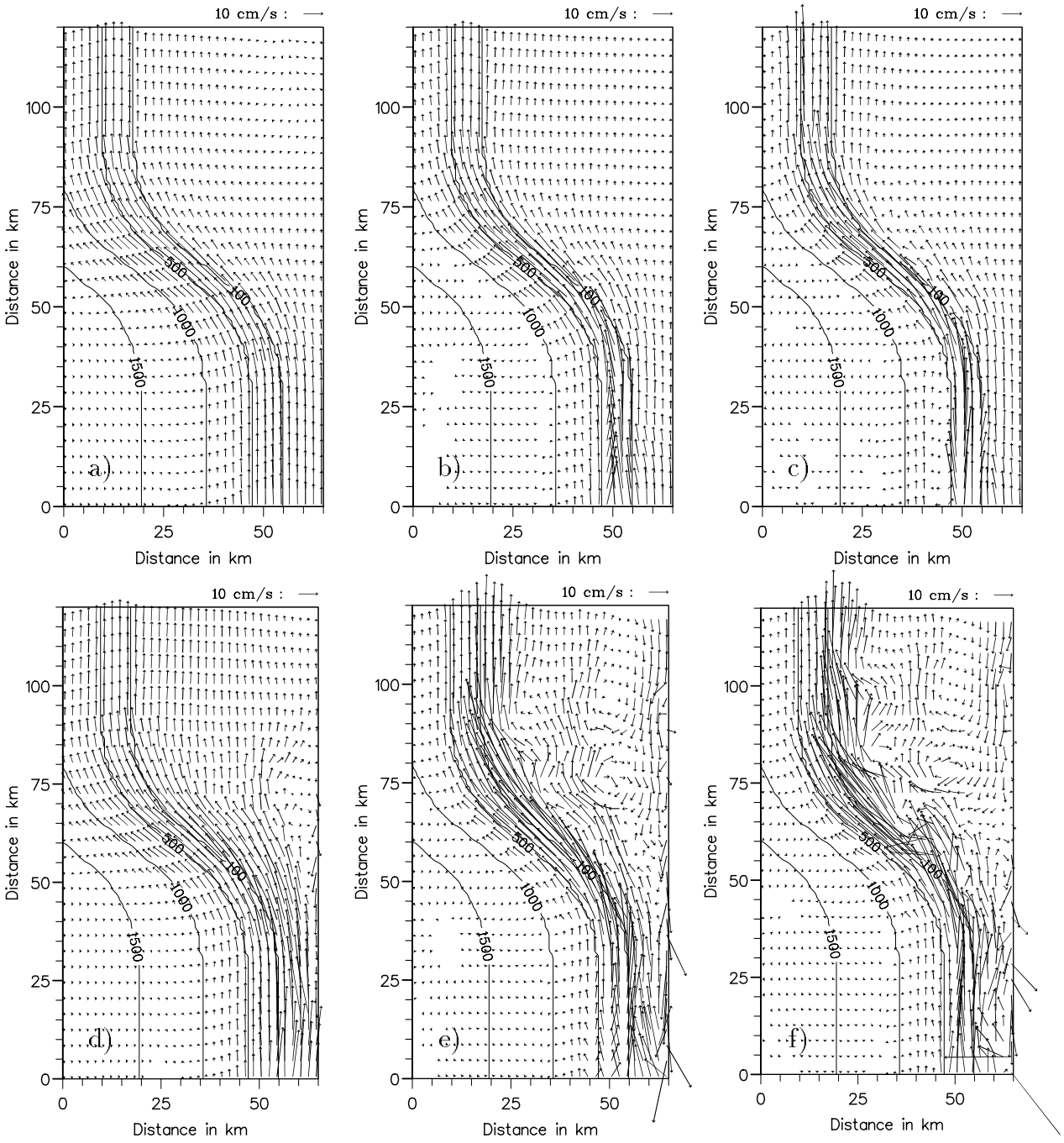

Figure 8. Topographic steering of a uniform current on the shelf and a sine shear layer on the shelf slope (eq. 13) with $u_0 = 0.2$ m/s, $B = 20$ km, L_B= 10 km. Shelf slope profile (eq. 7) with standard parameter values (table 1). Current fields near the transition zone at time 5, 10 and 15 days respectively left to right. (upper panel) and at time 5, 10 and 11 days for lower panel (unstable after 11 days). Depth contours for 100, 500, 1000 and 1500 m. Upper panel with bottom friction. Lower panel without bottom friction.

where $\kappa = \frac{1}{H}\frac{dH}{dy}$ must change sign (Collings and Grimshaw, 1980, Mysak, 1980). This criterion is derived under the frequently used assumption of a rigid lid at the surface which excludes the possibility of gravity wave modes. It may nevertheless provide useful information on the stability characteristics of the flows considered here and we have therefore used the criterion to estimate the stability bounds for typical current profiles. With the along shelf jet, (eq. 10), centered on the shelf slope, $B = S$ and $L_B = L + \frac{S}{2}$, we find

$$\frac{dQ}{dy} = -\frac{\kappa f}{H}\left[1 + \pi Ro \sin\frac{2\pi(y - L_B)}{B} - \frac{2\pi^2 Ro}{\kappa B}\cos\frac{2\pi(y - L_B)}{B}\right]$$

on the shelf slope. With uniform along shelf current on the shelf ($L_B = L$) and a sine shear layer on the slope, $B = S$, we find from (eq. 13):

$$\frac{dQ}{dy} = -\frac{\kappa f}{H}\left[1 + \frac{\pi Ro}{2}\cos\frac{\pi(y - L_B - \frac{B}{2})}{B} + \frac{\pi^2 Ro}{2\kappa B}\sin\frac{\pi(y - L_B - \frac{B}{2})}{B}\right]$$

where the Rossby number, $Ro = \frac{u_o}{fB}$, is based on the width of the current shear zone. This shows that $\frac{dQ}{dy}$ may change sign if $Ro > Min(\frac{1}{\pi}, \frac{\kappa B}{2\pi^2})$ for the jet profile. For the sine shear layer the similar critical value for the Rossby number is a factor 2-4 larger. Ohshima (1987) investigated the stability of a barotropic jet on a sloping bottom and calculated the growth rate and modal structure of unstable modes. This author found that the wave length of the most unstable modes are 2-3 times the width of the shelf slope and the e-folding time scale for growth is 1-3 days. For steep slopes the unstable modes are identified as shelf waves while for gentle slopes current shear becomes important. Ohshima also assumed periodic flow in the along shelf direction and calculated the exponential temporal growth rate of the waves. All his calculations are based on the rigid lid approximation. More recently Sheng (1995) has also investigated the stability of prograde and retrograde slope currents. Neither of these two studies apply directly to the condition on the Catalan shelf.

We have performed a series of numerical experiments in order to investigate the parameters governing the stability of a shelf edge current and the effect of topography on the flow. In the numerical experiments the current at the upstream (northeastern) boundary is either described as a jet with cosine profile (eq. 10 and 11) or as an uniform shelf current with a sine shear layer (eq. 13). This setup, which leads to a downstream spatial development of unstable modes, does not correspond exactly to the spatial periodic approach inherent in the formulation of the stability criterion (eq. 17). For this reason the results of the numerical simulations may not lead to the same stability bounds as deduced from the analytical expressions above. In the numerical model no assumption of rigid lid is made, and the available potential energy associated with the surface deformations and the propagation of surface gravity waves may therefore affect the stability of the flow.

The boundary conditions at the downstream end of the model domain are not very crucial to the interior solution as long as the boundary is far away. For most of the simulations, with a specified current inflow at the upstream boundary, we have implemented an uniform outflow at the downstream boundary with the same total volume

flux as upstream. In order to relax the interior solution to this boundary conditions we have use the FRS method. We have also tested other types of boundary conditions at the downstream boundary; no surface displacements, free current adjustment i.e. purely advective, no current i.e. rigid wall, a simple radiation condition (setting surface displacement $\eta = \frac{U\sqrt{H}}{\sqrt{g}}$), and a geostrophically balanced outflow based upon the current upstream. Finally we have also used enlarged simulation area. The conclusion of these tests is that the interior solution is not seriously affected by the boundary conditions.

Examples of flow instability and eddy development are shown by the results of two experiments displayed in figs. 9 and 10. In the first case the inflow at the upstream boundary is specified as wide jet centered outside the shelf edge. The corresponding potential vorticity is decreasing monotonically from the coastline towards the ocean with no secondary maximum on the shelf. According to the stability criterion above the flow should be stable, yet anticyclonic eddies develop on the narrow section of the shelf after about 5 days. The instability appears as short periodic shear flow instability within the jet near the upstream boundary with corresponding short periodic surface displacements. These disturbances evolve into larger scale eddy formation over shallow shelf. The eddies span the shallow shelf inside from the main jet and are slightly elongated in the along shelf direction, over a distance of about 20 km. The eddies propagate downstream with a speed of about 0.25 m/s and increase in strength. When the eddies encounter the transition zone between narrow and the broad section of the shelf a complex non-linear flow adjustment takes place. The anticyclonic eddies, upon propagating onto the wide section of the shelf, expand in a larger anticyclonic eddy structure which finally span the entire shelf width (fig. 9, a-c, upper panel). Intermittent in the adjustment process, before a new anticyclonic eddy approach the transition zone, a weak cyclonic eddy is also generated at the start of the transition zone (fig. 9, d, lower panel). This eddy also widens as it propagates onto the wider section of the shelf (e and f, lower panel) before a new anticyclonic eddy approaches the transition zone and the process recurs itself. A weak cyclonic eddy, with diameter about 20 km, is seen to develop on the seaside of the jet (fig. 9, a-c upper panel) and propagates slowly towards the transition zone where it dissolves. Eventually after about 15 days the eddy development becomes so vigorous that the simulation becomes numerically unstable. A control run without the advective terms in the momentum equation shows a stable smooth flow, topographically steered along the shelf edge in the transition zone, but with no eddies or tendencies for flow instability. This confirms that the eddies seen in (fig. 9) are the result of a non-linear instability process with energy transfer from the mean current to small scale eddies.

The sensitivity of the stability characteristics of the flow to small changes in the location of the jet relative to the shelf slope is seen by comparing the results in fig. 6 (lower panel) with these in fig. 9. With the center of the jet at the shelf edge (fig. 6) we see no strong tendency for formation of eddies on the narrow shelf, but a vigorous and complex eddy generation takes place on the broad section of the shelf near the transition zone. In this case (fig. 6) bottom friction effectively smooths the flow and prevents the formation of eddies on the shelf. The shelf edge flow, particularly on the

narrow section of the shelf does, however, contain an oscillatory component with period about 24 hours and amplitude about 10 % of the mean flow.

The simulations displayed in fig. 9, where bottom friction ($r_b = 0.003$) is included, shows that it is unable to prevent the formation of eddies in this case. An example to the opposite will be given by the next experiment which we will examine.

In the second case the inflow at the upstream boundary is specified as a narrow jet centered outside the shelf edge (fig. 10). The corresponding potential vorticity is decreasing monotonically from the coastline towards a minimum just beyond the shelf edge and with a well defined secondary maximum on the shelf slope. Hence, the flow is unstable according to the stability criterion and we see the development of eddies from about day 10, but the development is less vigorous than in the previous case. On the upstream narrow section of the shelf anticyclonic eddies appear slightly elongated in the along shelf direction, over a distance of about 20 km. In this case the eddies have a tendency to follow on the inside of the jet current which is being steered topographically along the shelf edge where the transition from the narrow to the broad shelf take place (fig. 10, a-c, upper panel). The strength of the eddies increases when they approach the transition zone. The induced anticyclonic circulation on the broad shelf is much weaker than in the previous case. Near the transition zone a small cyclonic eddy is seen to develop intermittently between the impinging anticyclonic eddies (fig. 10, d-e, lower panel)

In this latter case bottom friction is found to have a strong effect on the stability characteristics and the development of eddies and bottom friction will effectively reduce the eddy formation. This can be seen by comparing with fig. 7 also displaying results of simulations with the same shelf edge jet current.

Bottom friction is found to affect the flow mainly in two ways: firstly by reducing the flow speed downstream from the inflow boundary due to frictional damping, secondly by a direct damping effect by reducing the growth rate of unstable modes.

The effect of horizontal eddy viscosity on the flow has been investigated both with Smagorinsky type of eddy viscosity (Smagorinsky, 1963) and an ordinary constant eddy viscosity. Both methods leads to damping particularly of the short periodic fluctuations due to shear flow instability within the jet which occur for Rossby numbers around 0.1 and higher. The effect on the larger scale eddies seen to develop on the shelf is small. For example, for a cosine-jet (eq. 11) with $u_0 = 0.2$ m/s, $B = 10$ km, $L_B = 20$ km the amplitude of short periodic current oscillations (period 3-4 hours), which appear after about 10 days within the jet, are reduced by a factor 4-5 by increasing the eddy parameter q from 0.1 to 0.4. The relatively large short periodic surface displacements associateded with these current fluctuations are damped correspondingly. The larger scale eddy oscillations with period 2 days, which develop rapidly after the start of the event in this case, are little effected by this change in the magnitude of the horizontal viscosity.

For the same case we have also compared the results of the simulations with the three different numerical schemes as mention in section 5. Up to about 200 hours from start the three results are nearly identical, but the modified forward-backward and the leap-frog scheme (with $q = 0.1$) become unstable around 200 hours localized to an eddy in the transition zone between the narrow and the broad sections of the shelf.

The Heun scheme, which apparently is more dissipative, remains stable at least up to 360 hours and show the development of short periodic oscillations within the jet after 200 hours as described above.

9 Pulse inflow

The duration of the inflow have a considerable effect on the spatial and temporal structure of the downstream flow. An inflow event (fig. 11), is specified at the upstream boundary by eq. (15), and σ=$1.16 \cdot 10^{-5}\, s^{-1}$ which implies that the inflow reaches its maximum value after one day and tapers off to about 20 % of peak value after 4 days. Although relatively strong eddies develop on the shelf near the upstream boundary, eddy activity in the transition zone is less vigourous in this case. The tendency for topographic steering of the flow is nevertheless pronounced (fig. 11, b). A transient meandering counterflow is seen to develop on the broad section of the shelf near the transition zone from a broad to a narrow shelf after about 5 days with a quiet area near land (fig. 11, c). After about 7 days the flow has decayed.

10 Particle tracking

Figures 12-13 show drift of particles released in the unstable wide jet (fig. 9). In the first release (fig. 12) we also tagged the particles outside and inside the shelf edge with different colors (not shown here) to study the cross shelf drift. The part of the cluster initially located on the shallow shelf is strained but remains near the initial position. Particles initially located near or outside the shelf edge are transported by the topographically steered jet. The shape of the cluster is deformed into an elongated feature with cross shelf exchange taking place in the transition zone from the narrow to the broad shelf (fig. 12). The intrusion of shelf slope water onto the shelf is however limted to a zone near the 100 m depth contour.

Figure 13 shows particles released at the transition zone from a narrow to a broad shelf. There are strong mixing of the water masses near the 100 m contour, which is supported by structure of the current field displayed in figure 9. Particles released near the coastline experience a slow drift in upstream direction due to the prevailing anti-cyclonic circulation in the area. Plots with higher resolution of particle concentration (not shown) reveal patterns within the cluster which evidently are due to the eddy structures.

The displacement of the particles in cross and along shelf direction was also investigated by releasing particles from a point source (coordinate (138.3, 120), fig. 12) on the 100 meter isobath. The particles were released at intervals of 2 hours over a total time span of 100 hours, starting at t=100 hours in an experiment similar to that shown in fig. 9 and fig. 12. Each particle was subsequently traced for 360 hours. The displacement of the particles, measured by the distance along the 100 m isobath (along shelf displacement) and distance perpendicular to the same isobath (cross shelf displacement) was calculated and are displayed in fig. 14.

The spreading of the particles in cross shelf direction is limited within a region of

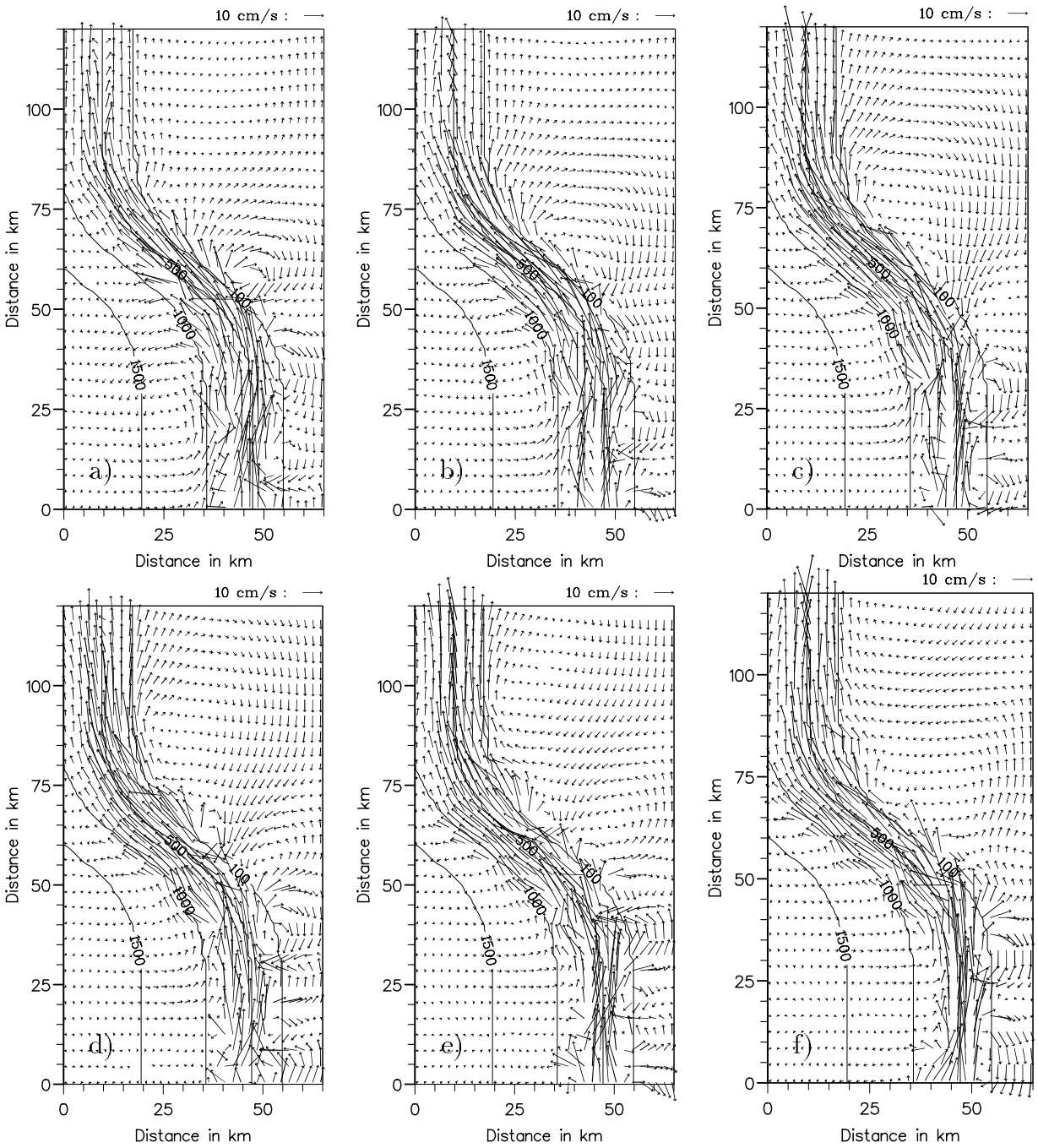

Figure 9. Unstable wide jet centered 10 km outside shelf break (eq. 11) with $u_0 = 0.2$ m/s, $B = 20$ km, $L_B = 20$ km. Shelf slope profile (eq. 7) with standard parameter values (table 1) with bottom friction. Current fields near the transition zone from day 12 with 12 hours consecutive intervals, ordered left-right top-bottom. Depth contours for 100, 500, 1000 and 1500 m.

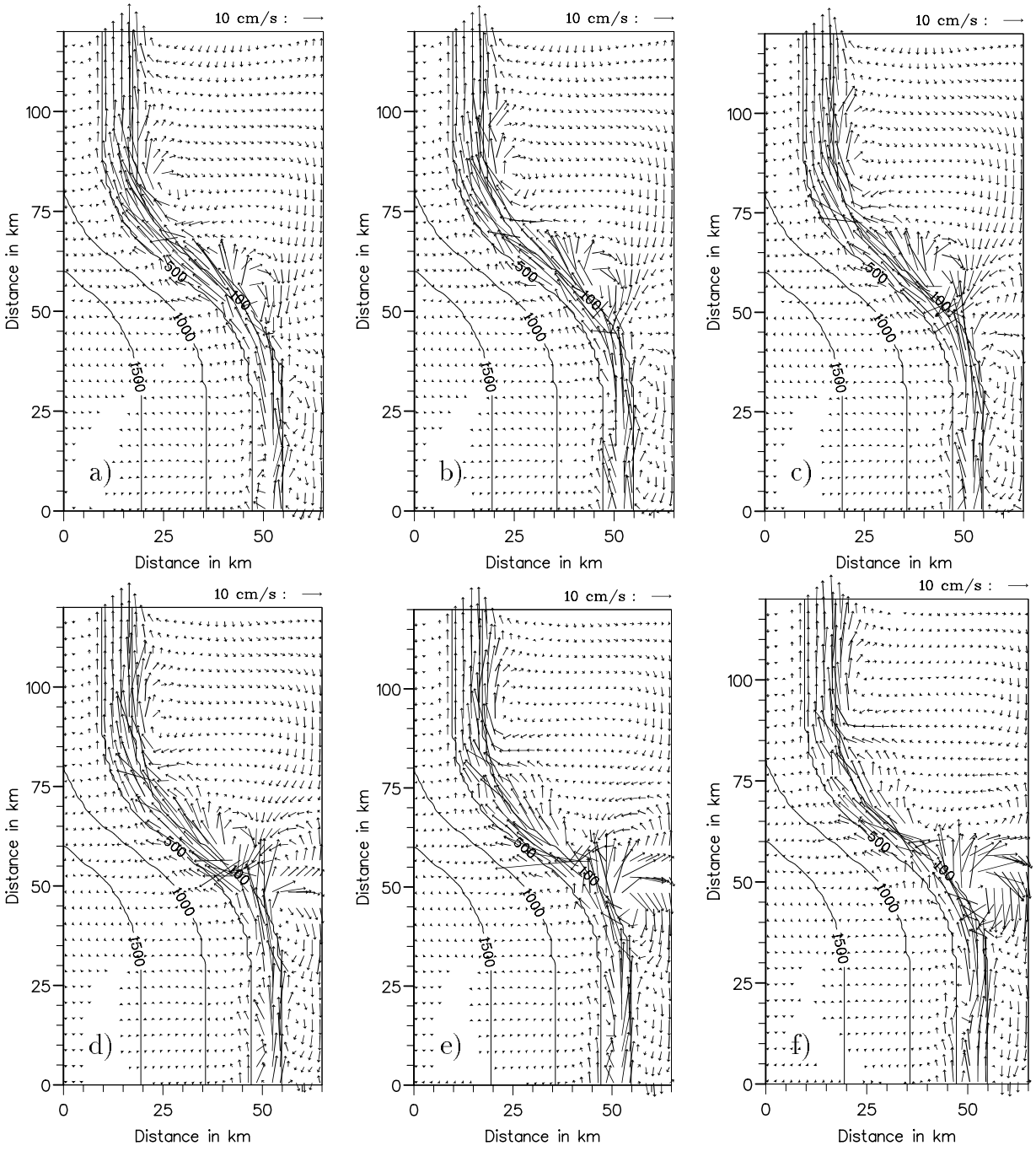

Figure 10. Unstable narrow jet centered 5 km outside shelf break (eq. 11) with $u_0 = 0.2$ m/s, $B = 10$ km, L_B= 15 km. Shelf slope profile (eq. 7) with standard parameter values (table 1) without bottom friction. Current fields near the transition zone at consecutive intervals of 6 hours from time 13.5 days (a,upper panel), ordered left-right top-bottom. (Current fields at 5, 10, and 15 days for the same case are shown in fig. 7). Depth contours for 100, 500, 1000 and 1500 m.

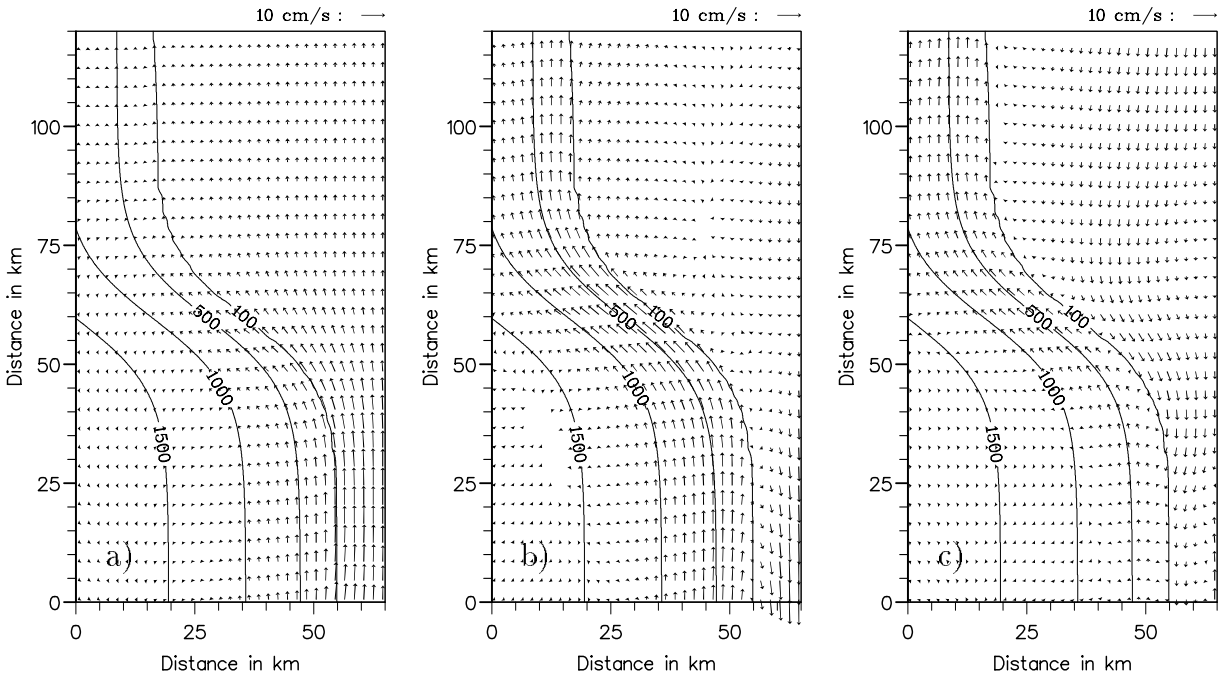

Figure 11. Pulse event with narrow jet centered 20 km outside shelf break (eq. 11) with $u_0 = 0.2$ m/s, $B = 10$ km, $L_B = 20$ km. Shelf slope profile (eq. 7) with standard parameter values (table 1) without bottom friction. Current fields near the transition zone at consecutive intervals of 2 days from day 2 (a), ordered left-right. Depth contours for 100, 500, 1000 and 1500 m.

about ± 10 km relative to the 100 m isobath. The spreading in along shelf direction ranges from 10 to 160 km at the end of the simulation. The cross shelf dispersion is caused mainly by the barotropic eddies occurring along the shelf edge. These eddies also have a considerable influence on the drift of particles in along shelf direction since they randomly delay particles in their along shelf drift. Diffusion coefficients were calculated from the formula

$$K_z = \frac{1}{2}\frac{d\sigma_z^2}{dt} \tag{18}$$

where σ_z^2 denotes the variance and z is a subscript for either *in cross shelf* or *along shelf* direction. Peak values of the diffusion coefficients were estimated to $1.6 \cdot 10^2$ m^2/s and $3.3 \cdot 10^3$ m^2/s in cross and along shelf direction respectively. The estimated diffusion coefficients vary considerable in time due to the complex eddy activity in the flow. Even negative dispersion coefficients appear describing convergence of the particles. The effective dispersion in both cross and along shelf direction is therefore much smaller than what these peak estimates indicate. Further details can be found in Ommundsen (1999).

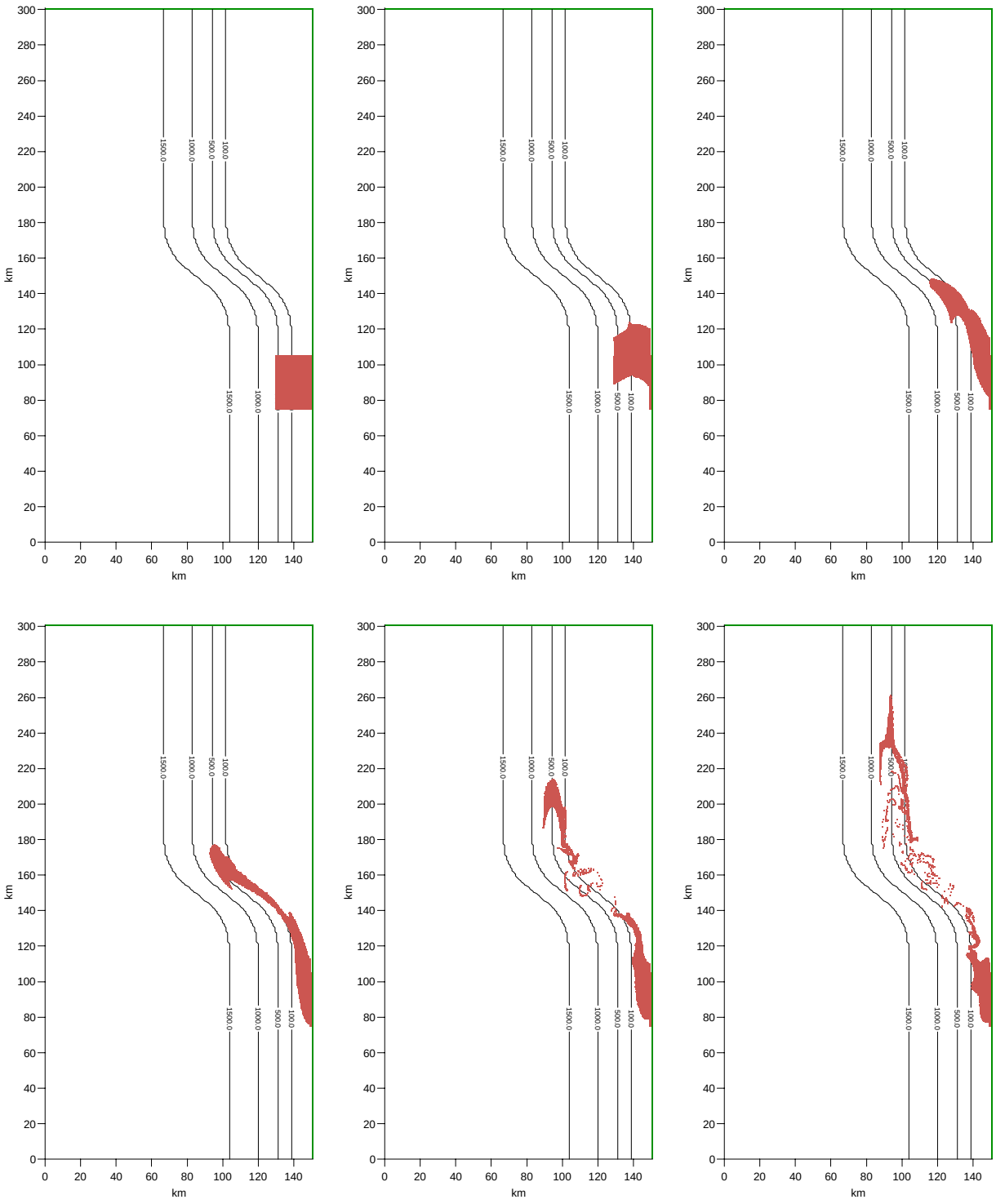

Figure 12. Particle tracking in wide jet (fig. 9). Particle location from initial release, $t = 0$, with 72 hours consecutive intervals, ordered left-right top-bottom. Total number of released particles 6767. Dark shading represent dense concentration of particles. Depth contours for 100, 500, 1000 and 1500 m.

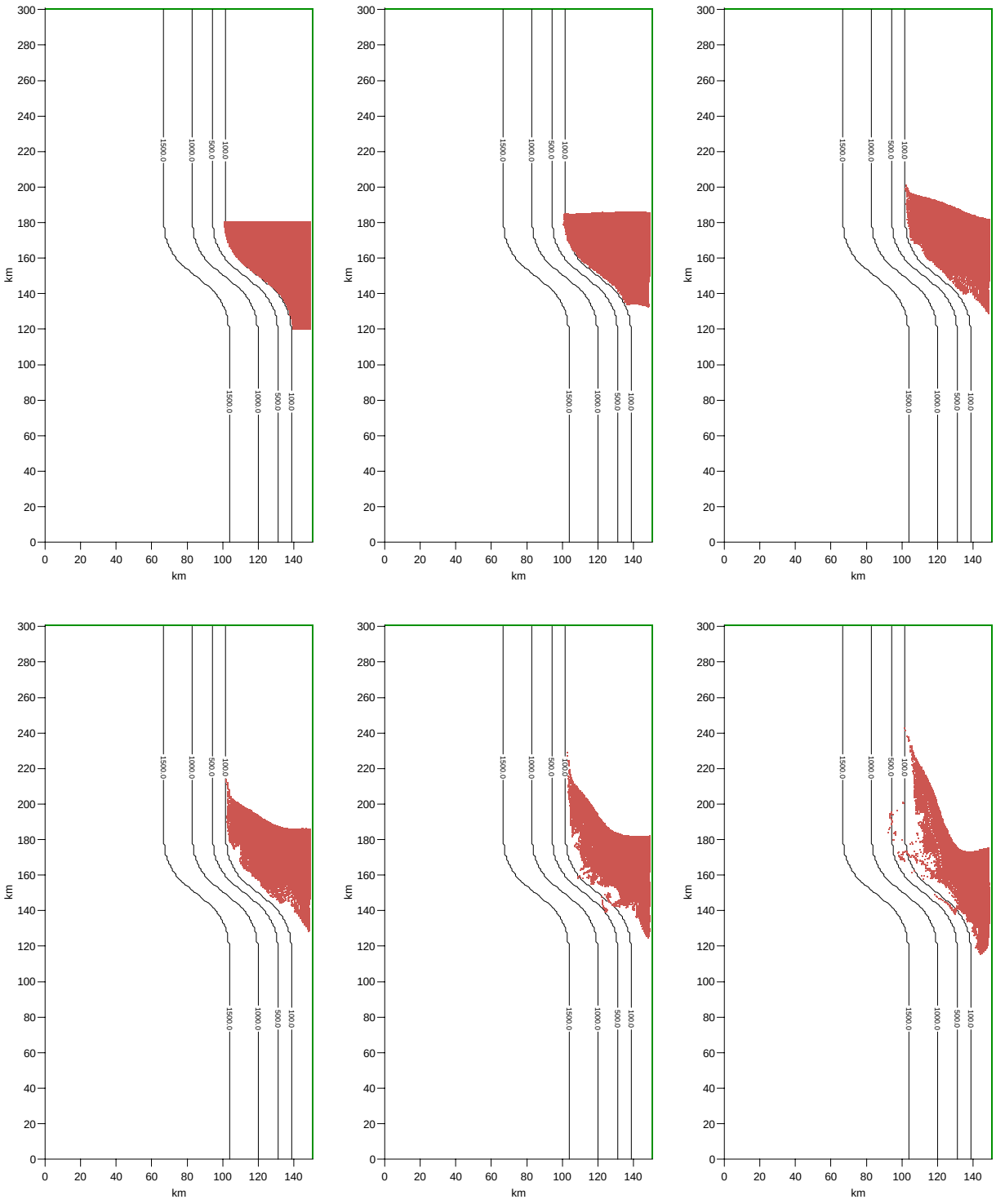

Figure 13. Particle tracking in wide jet (fig. 9). Particle location from initial release, $t = 0$, with 72 hours consecutive intervals, ordered left-right top-bottom. Total number of released particles 7175. Dark shading represent dense concentration of particles. Depth contours for 100, 500, 1000 and 1500 m.

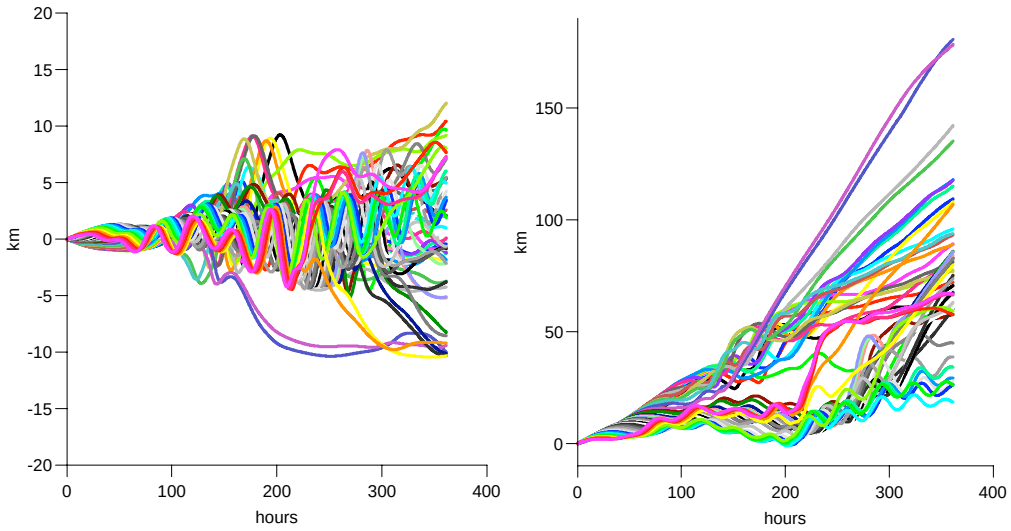

Figure 14. Left panel shows cross shelf displacement of particles relative 100 m isobath. Positive displacement is towards shallow water (depth<100 meter). Right panel shows along shelf displacement of particles on 100 m isobath. Positive displacement is towards the downstream boundary. Each particle traced for a time interval of 360 hours.

11 Eddy generation by wind forcing

During winter northwesterly wind events are common on the Catalan shelf and the strength is often enhanced by the wind channeling in the narrow lower Ebro valley (Font 1990). We have performed some numerical simulations with the idealized high resolution barotropic model described earlier in order to study the response of an offshore wind jet on the flow in the vicinity of the Ebro Delta. A previous study (Garcia et al., 1994) which used a coarser grid resolution did not properly resolve the transient atmospheric forcing and the ocean response.

The shear stresses at the surface (τ_{sx}, τ_{sy}) are modelled by a uniform background wind stress τ_o, in offshore direction, modulated by a jet with a cosine profile.

$$\tau_{sy} = \begin{cases} \tau_o s(t) \left[1 + \kappa \frac{1+\cos(2\pi \frac{x-x_o}{b})}{1+(\frac{y}{a})^2}\right], & -\frac{b}{2} \le x - x_o \le \frac{b}{2} \\ \tau_o s(t), & |x - x_o| > \frac{b}{2} \end{cases} \tag{19}$$

where a is a characteristic length scale for the decay in offshore direction, b is the width of the jet, which increases linearly with y i.e. $b = b_o[1 + (\frac{y}{a})]$ and κ is a dimensionless factor which specifies the strength of the jet relative to the background wind stress. The center axis of the wind stress jet is at $x = x_o$. The temporal variation of the wind stress is specified by the function (15), with $\sigma = 2.3 \cdot 10^{-5}\, s^{-1}$ the wind grew to a maximum in 12 hours, then tapered off gradually to 20 % of peak strength after 2 days and to only 4 % after 3 days. This wind stress model extends an earlier model by Han and Kohler (1983) for wind channeling due to terrain topography near the Ebro Delta.

The spatial distribution of the wind stress, one day after the start of the event is

shown in fig. 15 (a, upper panel). A typical feature of the current response to the wind forcing is the formation of a dipolar eddy structure as manifested by the plots of the depth mean current in fig. 15. The dipole axis is tilted at an angle of about 30 degrees relative to the axis of the wind jet. A strong current shear appears between the cyclonic and the anticyclonic eddy located on the narrow and broader part of the shelf respectively. A well defined flow separation point appears at the coast separating the two eddies. Up to 60 hours bottom friction has only a minor modifying effect on the flow pattern, mainly by reducing the current speed, as seen by comparing the results of the simulation with (fig. 15, b and c, upper panel) and without bottom friction (fig. 15, d and e, lower panel). Without bottom friction the strong current shear zone becomes unstable and at 120 hours a system of three eddies appears, two cyclonic and one anticyclonic. The diameter of the eddies are about 20 km and an almost symmetric dipolar eddy is seen to propagate downstream on the broad section of the shelf (not shown here). We have also performed simulations without horizontal eddy viscosity (q=0) and find that the flow field is little affected by horizontal eddy viscosity. In particular we find that the position of the flow separation point at the coast is almost unchanged. The along shelf variation in shelf width obviously has an effect particularly on the cyclonic eddy which is located over the narrow section of the shelf. We have also made simulations where the axis of the wind jet is shifted 15 km towards the broader section of the shelf, the jet still perpendicular to the coast. The dipole structure of the current response, with a flow separation point at the coast, is still evident, but the size of the eddy is affected (fig. 15, f, lower panel). This demonstrates the effect of the along shelf variation in shelf width on the wind forced eddy structure. Finally we have also performed simulation with reduced width of the wind jet (a = 20 km). Basically the same dipole eddy structure is seen to develop under the wind jet as seen in (fig. 15, d and e, lower panel), but the size of the eddies is reduced slightly with the center, particularly for the anticyclonic eddy, closer to the coastline.

12 Discussion and Conclusions

An important aspect has been to investigate the effects of shelf flow adjustment in the transition zone from a narrow to a broader shelf on the Catalan shelf northeast of the Ebro Delta. It has become evident that the simulated flows are very sensitive to small changes in the basic flow parameters with corresponding abrupt changes in the flow regime. It has therefore been crucial to document that the simulated flow fields reflects the physics and are not numerical artifacts. Comparative runs with a 2-D model based on a C-grid numerical scheme shows qualitatively similar flows (Xing and Davies, 2000), but a detail comparison of the performance of the B and the C-grid schemes for this particular problems will be addressed in a future study.

In light of this a large number of simulations have been performed with different numerical schemes, boundary conditions, and grid resolution down to 0.5 km in order to assess the accuracy of the numerical solutions. It has become clear that the wave instability and eddy formations seen in the simulations reflect the physics and that barotropic instability of the shelf edge current may be an actual mechanism for eddy

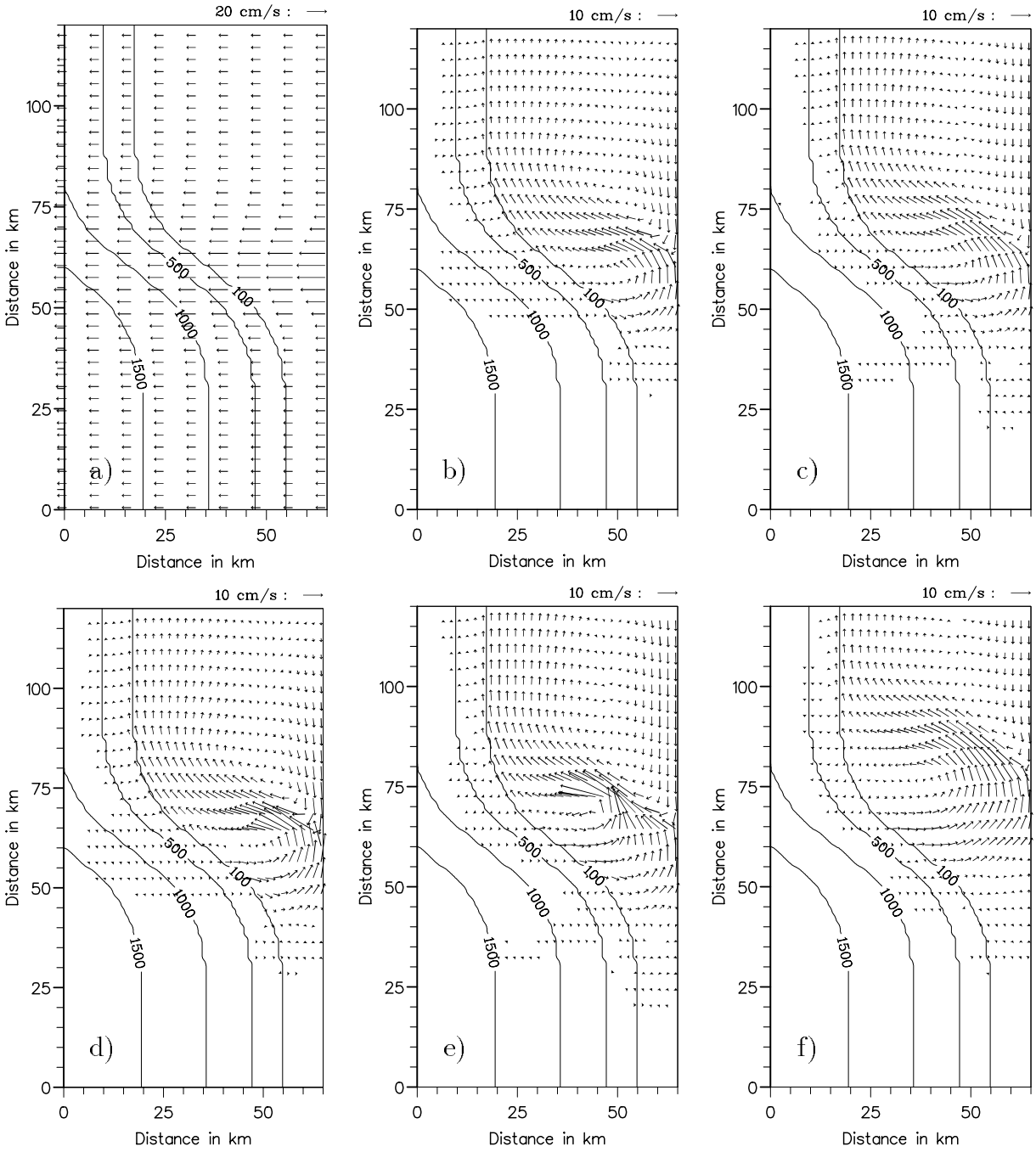

Figure 15. Forcing by wind jet (eq. 19) $\tau_o = 0.25$ Pa, $b = a = 30$ km, κ= 1.0. Shelf slope profile (eq. 7) with standard parameter values (table 1). Wind stress at time 1 day, upper panel a, with center of wind jet $x_o = 62.5$ km. Current fields near the transition zone with bottom friction at time 36 and 60 hours, respectively b and c, upper panel. Current fields without bottom friction at time 36 and 60 hours, respectively d and e, lower panel. Current field at 60 hours with the center of the wind jet shifted 15 km further down on the broad shelf, $x_o =$ 62.5 km, f, lower panel. Depth contours for 100, 500, 1000 and 1500 m.

formation on the Catalan shelf. It is also found that the along shelf current on the narrow section of the shelf has an important effect on the circulation and current structure in the transition zone to a broader shelf. A key quantity for the understanding of these processes is the potential vorticity of the flow. We find, however, that eddy formation may occur even if the current profile at the upstream boundary satisfies the stability criterion on the potential vorticity. Small changes in the strength and profile of the current at the upstream boundary may lead to completely different flow regimes downstream near the transition zone. In some cases the shelf edge flow tend to split in two branches at the transition zone; one follows the shelf break the other intrudes on the shallow broad shelf leading to the development of an anticyclonic eddy.

The most prominent features of the simulations are the strong tendency for topographic steering of the flow along the shelf edge in the transition zone from a narrow to a broader shelf. This effect is also found in the independent studies by Xing and Davies (2000). The steering develops on a time scale of 2-5 days for different upstream current profiles ranging from a narrow to a wide jet centered near the shelf edge and an uniform flow on the shelf. We find that bottom friction actually enhances the tendency to topographic steering by reducing the flow level and variability on the shallow shelf. To our knowledge this effect has previously not been documented.

Another important common feature of several of the simulated current fields is the tendency for development of a large anticyclonic eddy structure on the broad section of the shelf near the transition zone in shelf width. This leads to a weak upstream directed current near the coastline with associated cross shelf flow adjustments. The existence of this circulation cell is, however sensitive to bottom friction and with realistic values for the bottom friction coefficient the anticyclonic circulation is eroded except in cases with vigorous eddy generation on the narrow shelf upstream from the transition zone. Field measurements, also under FANS cruises, indicate the existence of an anticyclonic circulation on the shallow shelf near Ebro Delta. The persistence and stability of this circulation are not documented.

Calculations of dispersion properties and modal structure of barotropic shelf waves show that the broad shelf with relatively steep shelf slope southeast of the Ebro Delta may support wave oscillations with period down to about 24 hours. The maximum current associated with these oscillations is located near the shelf break with peak along and cross shelf components having nearly the same magnitude. Due to Doppler shift a steady along shelf jet with speed up to 0.25 m/s is capable of reducing the period down to about 20 hours which is close to the period of the current oscillations observed near the shelf break during the November 1997 FANS campaign. Unfortunately, the available data from the FANS cruises does not allow a systematic comparison with field data or an analysis of possible shelf wave oscillations in the area.

Acknowledgement This work has been financed by the Commission of European Communities under EU MAST-III project FANS contract MAS3-CT95-0037 and with a grant of computer time from Norwegian Research Council under National Program of Supercomputing.

References

Chapman, D. C., 1985. Numerical treatment of cross-shelf open boundaries in a barotropic coastal ocean model. Journal of Physical Oceanography 15, 1060–1075.

Collings, I. L., Grimshaw, R., 1980. The effect of topography on the stability of a barotropic coastal current. Dynamics of Athmospheres and Oceans 5, 83–106.

Font, J., 1990. A comparison of seasonal winds with currents on the continental slope of the catalan sea (northwestern mediterranean). Journal of Geophysical Research 95(C2), 1537–1545.

Font, J., Salat, J., Julia, A., 1990. Marine circulation along the ebo continental margin. Marine Geology 95, 165–177.

Garcia, E., Tintoré, J., Pinot, J., Font, J., Manriquez, M., 1994. Surface circulation and dynamics of the balearic sea. Seasonal and Interannual Variability of the Western Mediterranean Sea. Coastal and Estuarine Studies 46, 73–91.

García, M., Guillén, J., Palanques, A., Puig, P., Puigdefábregas, J., Sánches-Arcilla, A., 1997. Time series observations of currents across the ebro delta continental shelf and slope (november 1996-february 1997): Preliminary notes on shelf circulation. FANS Plenary Workshop, Blanes, Spain. Abstracts-in-depth, paper 1.8.

Gjevik, B., 1991. Simulations of shelf sea response due to travelling storms. Continental Shelf Research 11(2), 139–166.

Gjevik, B., Moe, H., 1994. Steady and transient flows around banks located near a shelf edge. Continental Shelf Research 14(12), 1389–1409.

Han, G., Kohler, K., 1982. Observed and modelled circulation on the Spanish Mediterranean continental shelf near Rio Ebro. Science Application Inc., Miami, Fla. Rep. NA82RAC000222, 70p.

Haugan, P. M., Evensen, G., Johannessen, J. A., Johannessen, O. M., Pettersson, L. H., 1991. Modelled and observed mesoscale circulation and wave-current refraction during the 1988 norwegian continental shelf experiment. Journal of Geophysical Research 96(C6), 10487–10506.

Hill, A. E., 1995. Leakage of barotropic slope currents onto the continental shelf. Journal of Physical Oceanography 25, 1617–1621.

Huthnance, J. M., 1981. Waves and currents near the continental shelf edge, Progress in Oceanography 10, 193–226.

Huthnance, J. M., 1987. Effects of longshore shelf variations on barotropic continental shelf waves, slope currents and ocean modes. Progress in Oceanography 19, 177–220.

Huthnance, J. M., 1995. Circulation, exchanges and water masses at the ocean margin: the role of physical processes at the shelf edge. Progress in Oceanography 35, 353–431.

Kajiura, K., 1974. Effect of stratification on long period trapped waves on the shelf. Journal of the Oceanographical Society of Japan 30, 271–281.

La Violette, P. E., Tintoré, J., Font, J., 1990. The surface circulation of the balearic sea. Journal of Geophysical Research 95(C2), 1559–1568.

Martinsen, E. A., Engedahl, H., 1987. Implementation and testing of a lateral boundary scheme as an open boundary condition in a barotropic ocean model. Coastal Engineering 11, 603–627.

Mesinger, F., Arakawa, A., 1976. Numerical methods used in atmospheric models. GARP Publ. ser. WMO 17, 64 pp.

Mysak, L. A., 1980. Recent advances in shelf wave dynamics. Review of Geophysics and Space Physics 18(1), 211–241.

Narayanan, S., Webster, I., 1987. Coastally trapped waves in the presence of a barotropic shelf edge jet. Journal of Geophysical Research 92(C9), 9494–9502.

Ohshima, K. I., 1987. Stability of a barotropic jet on a sloping bottom. Journal of the Oceanographical Society of Japan 43, 49–60.

Ommundsen, A., 1999. Particle Tracking in Idealized Barotropic Flow on the Catalan Shelf. Preprint Series, Department of Mathematics, University of Oslo. (http://www.math.uio.no/eprint/appl_math/1999/appl_1999.html)

Press, W. H., Flannery, B. P., Teukolsky, S. A., Vetterling, W. T., 1989. Numerical Recipes. Cambridge University Press, Cambridge.

Rippeth, T. P., Simpson, J. H., Player, R. J., and Garcia, M., 2000. Current oscillations in the diurnal-inertial band on the Catalunyan Shelf. Continental Shelf Research This volume.

Salat, J., Tintoré, J., Font, J., Wang, D. P., Vieira, M., 1992. Near-inertial motion on the shelf-slope front off northeast spain. Journal of Geophysical Research 97(C5), 7277–7281.

Sheng, L., 1995. The dynamics of a slope current in the Barents Sea. Near-Inertial Motion on the Shelf-Slope Front off Northeast Spain. Dr. ing. dissertation, Department of Structural Engineering, NTNU, Trondheim, Norway. ISBN 82-7119-860-2, 141 p.

Smagorinsky, J., 1963. General circulation experiments with the primitive equations. Monthly Weather Review 91(1), 99–164.

Tintoré, J., Wang. D. P., La Violette, P. E., 1990. Eddies and thermohaline intrutions of the shelf/slope front off thenortheast spanish coast. Journal of Geophysical Research 95(C2), 1627–1633.

Wang, D. P., Vieira, M. E. C., Salat, J., Tintoré, J., La Violette, P. E. 1988. A shelf/slope frontal filament off the northeast spanish coast. Journal of Marine Research 46, 321–332.

Webster, I., 1987. Scattering of coastally trapped waves by changes in continental shelf width. Journal of Physical Oceanography 17, 928–937.

Wilkin, J. L., Chapman, D. C., 1987. Scattering of continental shelf waves at a discontinuity in shelf width. Journal of Physical Oceanography 17, 713–724.

Willmot, A. J., Collings, I. L., 1994. Steady, frictionally modified wind and current forced shelf circulation: Application to vancouver island. Continental Shelf Research 14(12), 1601–1620.

Xing, J., Davies, A. M., 2000. Influence of long shelf topography upon cross shelf exchange and flow stability in the region of the Ebro Delta. Submitted to Continental shelf Research.

Yankovsky, A. E., Chapman, D. C., 1997. Anticyclonic eddies trapped on the continental shelf by topographic irregularities. Journal of Geophysical Research 102(C3), 5625–5639.